



Modelling Rock Failure with a Novel Continuous to Discontinuous Method

Bin Gong^{1,2} · Shanyong Wang¹ · Scott William Sloan¹ · Daichao Sheng³ · Chun'an Tang²

Received: 6 August 2018 / Accepted: 6 February 2019 / Published online: 20 February 2019
© Springer-Verlag GmbH Austria, part of Springer Nature 2019

Abstract

The original discontinuous deformation and displacement (DDD) method is greatly refined using the statistical damage theory and contact mechanics. Next, a novel coupled method is proposed to model the continuous to discontinuous failure process of rocks. By hybridizing the finite element method (FEM) and discontinuous deformation analysis (DDA) method, the proposed method inherits the advantages of both and is able to provide a complete and unified description of rock deformation, crack initiation and propagation, and rock body translation, rotation and interaction. Moreover, to improve the deformation results and refine the stress distribution within the model blocks, finite elements are introduced into the blocks. The ability of an intact block to fracture is included as well, i.e., the deformable blocks that contain several finite elements may split into smaller blocks if the strength criteria are satisfied continuously. The boundaries of damaged elements represent newly formed joints, and sliding and opening may occur along these joints, i.e., mechanical interaction is allowed between adjacent blocks. The correctness and validity of the proposed method are verified through a series of benchmark tests. The simulated results are consistent with the analytical solutions, previous studies and experimental observations. Overall, the coupled method is an effective and reliable approach for modelling the entire rock failure process with satisfactory accuracy and shows considerable potential in geotechnical engineering.

Keywords Rock failure · Whole-process analysis · Discontinuous deformation analysis · Numerical simulation

List of Symbols

d_i	A 2×1 displacement sub-matrix	K_{ij}	A 2×2 coefficient sub-matrix
E	Elastic modulus of the damaged material element	m	Homogeneity index
E_0	Elastic modulus of the undamaged material element	P	Diametral loading
f_{c0}	Uniaxial compressive strength	R	Radius of the specimen
f_{cr}	Residual compressive strength	t	Time or thickness of the specimen
f_{t0}	Uniaxial tensile strength	u	Parameter of an element
f_{tr}	Residual tensile strength	u_0	Scale parameter related to the mean value of the element parameter
F_i	A 2×1 external loading sub-matrix	$\{u_i, v_i\}^T$	Translations of node i along the x - and y -axes
g	Gravity acceleration	u_x, u_y	Block displacement along the x and y -axes
		w_i	Any component of (u_i, v_i)
		(x, y)	Point coordinates
		α	Half of the loading angle
		σ_x, σ_y	Normal stresses along the x - and y -axes, respectively
		$\sigma_1, \sigma_2, \sigma_3$	Major, intermediate and minor principal stresses, respectively
		$\varepsilon_1, \varepsilon_2, \varepsilon_3$	Major, intermediate and minor principal strains, respectively
		ε_{c0}	Compressive threshold strain
		ε_{t0}	Elastic limit strain (or tensile threshold strain)
		ε_{tu}	Ultimate tensile strain

✉ Shanyong Wang
Shanyong.Wang@newcastle.edu.au

¹ Faculty of Engineering and Building Environment, Priority Research Centre for Geotechnical Science & Engineering, The University of Newcastle, Callaghan, Australia

² Faculty of Infrastructure Engineering, Dalian University of Technology, Dalian 116024, China

³ School of Civil & Environmental Engineering, University of Technology Sydney, Sydney, Australia

η	Ultimate strain coefficient
θ	Dip angle of the slope
λ	Residual strength coefficient
μ	Poisson's ratio
ρ	Density of the rock material
φ	Internal friction angle
ω	Damage variable

1 Introduction

The safety and stability of rock engineering is an unavoidable problem in infrastructure construction. The existence of discontinuities in a rock mass has made this topic challenging in terms of evaluating the rock mechanics. Naturally, as a discontinuous material, a rock mass generally contains multiple joints and fractures (Hudson and Harrison 1997). The behavior of a rock mass has been recognized to be significantly affected by the formation of complex discontinuities. These potential instabilities are dominated by the physical and mechanical parameters of both the rock matrix and its discontinuities. Regarding either microcracks or macrojoints, these fractures normally initiate at weak points, such as voids, grain boundaries, faults, and other fractures. When assessing the complex microstructures of rock material, traditional analytical methods are invalid. Therefore, effective computational methods are needed for modelling rock masses and reproducing the rock failure process.

In recent decades, numerical techniques have become promising tools for research because of the development of computational mechanics and computer science; more specifically, various numerical methods have been developed to study the nonlinear deformation and failure behavior of rocks. Current numerical methods are commonly categorized into three main groups, i.e., continuous methods, discrete methods and hybrid methods (Jing 2003). The finite element method (FEM) (Rutqvist et al. 2001), the finite difference or volume method (FDM/FVM) (Fallah et al. 2000), the boundary element method (BEM) (Brady and Bray 1978) and the extended or generalized FEM (XFEM/GFEM) (Strouboulis et al. 2000) are representative continuous methods that have been applied to study a wide variety of situations. However, multiple joint sets that govern the mechanical behavior of a rock mass cannot be easily simulated by traditional continuum-based methods. The distinct element method (DEM) proposed by Cundall (1971) and the discontinuous deformation analysis (DDA) proposed by Shi (1988) are two mainstream discrete methods used in rock engineering. DEM discretizes the computational domain into separate blocks or particles, and then an explicit time-domain integration scheme is applied to solve the motion equations for the contactable discrete bodies. The particle-based DEM is able to model the granular microstructure

of rock-like materials. In this approach, the mechanical interaction between adjacent particles is allowed, and the determination of a contact is relatively simple. The block-based DEM assigns a normal stiffness and a tangential stiffness to the contacts between adjacent blocks. The stress, strain and displacement within a divided block can be calculated using a finite difference scheme (Barla et al. 2012). DDA is regarded as an implicit block-based DEM by some researchers (Jing and Stephansson 2007). The implicit solution scheme of DDA makes it unconditionally stable with any time step; it is even reasonable for a relatively large time step. As a discrete technique, the DDA method can simultaneously address the translation, rotation and deformation of divided blocks as well as the detachment and sliding along block boundaries using a unified computational format. Similar to FEM, the governing equation of DDA is expressed by a set of linear equations obtained by minimizing the total potential energy of the entire system. Moreover, the energy dissipation in DDA is mainly caused by friction and algorithmic damping, and additional damping is not required. The DDA has already been applied in many aspects of rock mechanics (Ning and Zhao 2013; Bao and Zhao 2013; Jiao et al. 2012).

The realistic failure process analysis (RFPA) (Tang 1997; Liang et al. 2004) was developed based on continuum mechanics to simulate the process of crack initiation, propagation and coalescence that occurs during the small-deformation stage of rock-like quasi-brittle materials. Since it was first proposed by Tang (1997), the RFPA code has been widely used in many engineering fields (Tang and Hudson 2002; Wang et al. 2011; Li et al. 2015). As a FEM-based method, RFPA is able to simulate fracture development with no prior assumptions regarding where and how cracks and other forms of failure are generated and is effective when considering multiple joint sets. However, RFPA cannot be used to model the block contacting, detaching, sliding and toppling processes that could be easily simulated by the DDA method. To address this issue, the discontinuous deformation and displacement analysis (DDD) method was proposed by Tang et al. (2015). By combining the FEM and DDA, and taking advantage of both methods, the DDD method has the capability to model continuous to discontinuous processes from the small-deformation stage to the large-displacement stage. Gong and Tang (2016) applied this approach to reproduce the evolution of a rock slope slide that occurred in the Alpetto Mine (Italy) in 1997 and confirmed its validity for use in calculating the rock fracture initiation, propagation, and coalescence and ultimately landsliding. Gong et al. (2018) introduced the gravity increase method (GIM) into the original DDD code to study coastal cliff recession. The complete failure processes of the gravity-induced collapses of notched rocky cliffs were modelled, and the instability mechanism was discussed.

In the original DDD code, the computational domain is separated into the RFPA domain and the DDA domain on the basis of the large-displacement criterion, as shown in Fig. 1. The large-displacement elements will appear with the formation of a failure surface. The failure surface will gradually form due to crack initiation and propagation, as calculated by the RFPA module. Afterwards, these large-displacement elements will automatically be translated into new blocks for the DDA module. Each element corresponds to one block. Mechanical interactions between different blocks are permitted, and the contact force between the boundaries of the two main domains is calculated according to the contact mechanics, i.e., the DDA domain does not contain any finite element, and the RFPA domain does not contain any blocks. Thus, the previous code is more suitable for modelling slope sliding or toppling collapses in the case that obvious failure surfaces form and large-displacement bodies are generated; this characteristic may limit the further development of the DDD method.

In this paper, the original DDD code is greatly refined using statistical damage theory (Krajcinovic and Silva 1982) and contact mechanics (Shi 2015). Then, a novel coupled method is proposed. As a continuous to discontinuous method, the proposed method inherits the advantages of the previously described methods. Moreover, by hybridizing the FEM and DDA methods, the proposed method can provide a complete and unified description of the whole rock deformation (including crack initiation and propagation) and rock body movement (including translation, rotation and interaction). Deformable bodies that contain several finite elements may be formed during the modelling process, according to the strength criteria. The deformation and stress distribution within rock bodies are, therefore, improved because the stress and strain obtained in one block are constant in the standard DDA formulation. Even the standard DDA approach is acceptable when reducing the size of a single block; however, using this approach will increase the computation time considerably. In addition, the formed rock bodies will split into smaller pieces if the strength criteria are satisfied continuously. These enhancements will

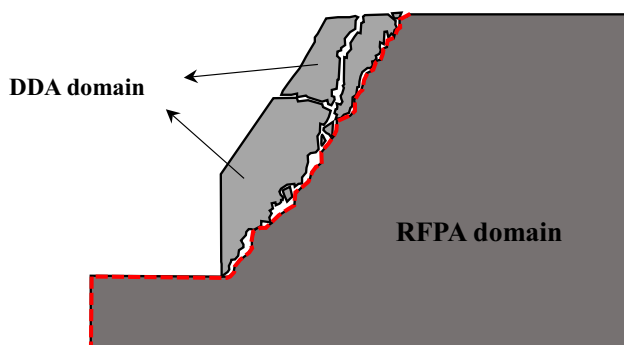


Fig. 1 Schematic of the original DDD method (dashed line represents the boundary between the RFPA and DDA domains)

definitely extend the DDD application range. Moreover, a series of numerical benchmarks are conducted in this study, and the correctness and validity of the novel coupled method are discussed. Note that, in the present study, the proposed method and related numerical simulations are based on the two-dimensional level.

2 Theory of the Coupled Method

2.1 Assignment of the Material Properties

Heterogeneity is one of the major characteristics of a rock mass, and it has a great influence on the failure process and failure modes of rock-like materials (Manthei 2005). According to statistical damage theory, the geotechnical structure is assumed to consist of many representative volume elements (RVEs), and the mechanical properties of these elements conform to a given distribution function. The Weibull distribution is regarded as a reasonable function that can be used to express the parameter distribution of quasi-brittle materials (Weibull 1951; Basu et al. 2009). Thus, for elements of a similar size in the proposed method, the values of a mechanical parameter are assumed to obey a given Weibull distribution, as defined in the following probability density function (PDF) (Weibull 1951):

$$f(u) = \frac{m}{u_0} \left(\frac{u}{u_0} \right)^{m-1} \exp \left(- \frac{u}{u_0} \right)^m, \quad (1)$$

where u is the parameter of the RVEs (e.g., elastic modulus or cohesion), u_0 a scale parameter related to the mean value of the parameter u , and m defines the basic shape of the given PDF. Considering that m represents the degree of heterogeneity in the material, it is generally termed the homogeneity index. A greater value of m (> 1) indicates a more homogeneous material, and vice versa. Hence, a heterogeneous numerical specimen can be produced computationally using a specific PDF.

2.2 The Constitutive Relation of a RVE

Initially, all finite elements are considered to be elastic, and their elastic properties are expressed by Young's modulus and Poisson's ratio. In particular, the constitutive model for each element is considered to be linearly elastic until the given damage thresholds are attained. Subsequently, the element is modified by softening. Related studies have indicated that the cracking process usually cannot be represented simply by either the tensile crack opening evolution or the crack sliding evolution (Hoxha and Homand 2000), and the tensile opening and shearing mechanisms show obvious advantages over other crack

evolution mechanisms (Meglis et al. 1995). Hence, the Mohr–Coulomb criterion with a tension cut-off is chosen as the strength criterion to capture the principal rock damage and fracture modes. Considering that microscale fractures represent the fundamental damage process, the maximum tensile strain criterion will be applied preferentially.

In elastic damage mechanics, considering the concept of modified effective stress, the elastic modulus of each element degrades monotonically as damage evolves. The damage variable ω ($0 \leq \omega \leq 1$) is defined as follows (Tang et al. 2015):

$$E = (1 - \omega)E_0, \quad (2)$$

where E and E_0 represent the elastic modulus of the damaged and undamaged material elements, respectively. Moreover, in the current study, the element and related damage are assumed to be isotropic and elastic.

When the finite element is subjected to a uniaxial tensile stress state, the stress–strain curve is linear-elastic, and no damage occurs in the beginning of the simulation, i.e., the damage variable $\omega = 0$. Tensile damage will occur when the maximum tensile strain criterion is reached; then, the parameter ω can be described as follows (Tang et al. 2015):

$$\omega = \begin{cases} 0 & \varepsilon > \varepsilon_{t0} \\ 1 - \frac{\lambda \varepsilon_{t0}}{\varepsilon} & \varepsilon_{tu} < \varepsilon \leq \varepsilon_{t0} \\ 1 & \varepsilon \leq \varepsilon_{tu} \end{cases}, \quad (3)$$

where λ represents the coefficient of residual strength, which can be given as $f_{tr} = \lambda f_{t0} = \lambda E_0 \varepsilon_{t0}$ (where f_{t0} and f_{tr} are the uniaxial tensile strength and the residual tensile strength, respectively); ε_{t0} represents the elastic limit strain and is termed the threshold strain; and ε_{tu} represents the ultimate tensile strain at which the element will be fully damaged. ε_{tu} can be defined as $\varepsilon_{tu} = \eta \varepsilon_{t0}$, where η is termed the ultimate strain coefficient.

When an element is subjected to a multiaxial stress state, it will be damaged in the tensile mode when the equivalent principal tensile strain $\bar{\varepsilon}$ reaches the abovementioned threshold strain ε_{t0} . $\bar{\varepsilon}$ is determined by

$$\bar{\varepsilon} = -\sqrt{\varepsilon_1^2 + \varepsilon_2^2 + \varepsilon_3^2}, \quad (4)$$

where ε_1 , ε_2 and ε_3 represent the major, intermediate and minor principal strains, respectively. The operator $\langle \rangle$ is defined as follows:

$$x = \begin{cases} x & x \leq 0 \\ 0 & x > 0 \end{cases}. \quad (5)$$

Additionally, when a finite element is under a compressive-shear stress state, the Mohr–Coulomb criterion

is chosen to determine the damage threshold of the shear failure and is expressed as follows (Tang et al. 2015):

$$f_{c0} \leq \sigma_1 - \frac{1 + \sin \varphi}{1 - \sin \varphi} \sigma_3, \quad (6)$$

where σ_1 represents the major principal stress and σ_3 represents the minor principal stress. φ and f_{c0} are the internal friction angle and uniaxial compressive strength, respectively.

When an element is subjected to a uniaxial compression stress state and becomes damaged according to the Mohr–Coulomb criterion, the damage variable ω can be expressed as follows (Tang et al. 2015):

$$\omega = \begin{cases} 0 & \varepsilon < \varepsilon_{c0} \\ 1 - \frac{\lambda \varepsilon_{c0}}{\varepsilon} & \varepsilon \geq \varepsilon_{c0} \end{cases}, \quad (7)$$

where λ represents the coefficient of residual strength, which can be given as $f_{cr} = \lambda f_{c0} = \lambda E_0 \varepsilon_{c0}$ (where f_{c0} and f_{cr} are the uniaxial compressive strength and the residual compressive strength, respectively); and ε_{c0} represents the compressive threshold strain.

In a multiaxial stress state, if the strength of an element satisfies the Mohr–Coulomb criterion, then tensile damage will occur. The compressive threshold strain ε_{c0} can be calculated at the peak strength and can be expressed as follows (Tang et al. 2015):

$$\varepsilon_{c0} = \frac{1}{E_0} \left[f_{c0} + \frac{1 + \sin \varphi}{1 - \sin \varphi} \sigma_3 - \mu(\sigma_1 + \sigma_2) \right]. \quad (8)$$

In the current method, it is assumed that the shear damage evolution is determined by only the maximum compressive principal strain, ε_1 , i.e., the element strain ε is replaced by ε_1 under triaxial stress states when testing the Mohr–Coulomb criterion.

2.3 Hybridization of the FEM and DDA

In the proposed method, conventional triangular elements are used to build the models because any polygon (either convex or concave) can be discretized by triangles. The formulations of the proposed method are constructed on the basis of the principle of minimization of the total potential energy, and the kinematics are fully inherited from the original DDA method. Unlike in the standard DDA, in the new method, the basic solving objects are the triangular elements, and their nodal displacements are the basic unknowns. In the standard DDA method, the basic unknowns are the three displacement components and the three strain components that are independent of block shape; thus, the stress and strain distributions inside a block are constant. When the block size is relatively small, this shortcoming may be acceptable; however,

reducing the block size may increase the computation time, limiting many engineering applications. As a coupled FEM/DDA algorithm, the proposed method will improve the accuracy of the deformation and stress distribution inside blocks by introducing finite elements into the blocks without losing any advantages of the standard DDA method.

As basic unknowns, the displacements are obtained at each node by solving the global equilibrium equation; in this process, the continuous and discontinuous regions are unified in analysis. Next, the strain and stress components are determined for each element. Simultaneously, the damage judgement module is used to determine whether a finite element is damaged in a tensile mode or shear mode during a certain loading step. When the failure criteria are satisfied, an element will be considered damaged. Note that newly damaged elements will cause a redistribution of stress, which is executed using the updated parameter values under the same loading conditions, and the damage judgement module will be rerun until no additional damage appears. Then, the next loading step is applied. The stress redistribution caused by a damaged element may induce additional damage to the adjacent elements; thus, macrocracks and fractures may occur because of the coalescence of the damaged finite elements.

By minimizing the total potential energy of the system, the global equilibrium equations can be generated as follows:

$$\begin{bmatrix} K_{11} & K_{12} & \cdots & K_{1n} \\ K_{21} & K_{22} & \cdots & K_{2n} \\ \vdots & \vdots & \ddots & \vdots \\ K_{n1} & K_{n2} & \cdots & K_{nn} \end{bmatrix} \begin{Bmatrix} d_1 \\ d_2 \\ \vdots \\ d_n \end{Bmatrix} = \begin{Bmatrix} F_1 \\ F_2 \\ \vdots \\ F_n \end{Bmatrix}, \tag{9}$$

where K_{ij} is a 2×2 sub-matrix, F_i is the external loading sub-matrix, and d_i is the displacement sub-matrix of node i , which contains two components $\{u_i, v_i\}^T$. u_i and v_i are the translations of node i along the x - and y -axes, respectively. Because triangular elements are used in the present method, the six displacement components of Element p can be listed as a vector:

$$D_p = \begin{Bmatrix} d_i \\ d_j \\ d_m \end{Bmatrix}. \tag{10}$$

If w_i represents any component of (u_i, v_i) , then the displacement at point (x, y) within element p can be calculated by the following equations:

$$w_{(x,y)} = \frac{1}{2\Delta} \begin{pmatrix} 1 & x & y \end{pmatrix} \begin{bmatrix} x_j y_m - x_m y_j & x_m y_i - x_i y_m & x_i y_j - x_j y_i \\ y_j - y_m & y_m - y_i & y_i - y_j \\ x_m - x_j & x_i - x_m & x_j - x_i \end{bmatrix} \begin{Bmatrix} w_i \\ w_j \\ w_m \end{Bmatrix}. \tag{11}$$

The symbol Δ is expressed as follows:

$$\Delta = \frac{1}{2} \begin{vmatrix} 1 & x_i & y_i \\ 1 & x_j & y_j \\ 1 & x_m & y_m \end{vmatrix}. \tag{12}$$

2.4 Improvements to the Original DDD Code

In the original DDD code, the analysis region is divided into the DDA domain and the FEM domain during calculation, according to the large-displacement criterion and is, therefore, suitable for simulating instabilities in nature or engineering that involve large-displacement processes, such as slope sliding or toppling. However, the stress and strain distributions within a single block in the DDA domain are constant. Such distributions may be acceptable if the block size is small enough; however, to attain a satisfactory result, decreasing the average block size will reduce the computational efficiency considerably. Moreover, although DDA can handle pre-existing discontinuities, the blocks in DDA are undividable, i.e., the initiation and propagation of a crack inside a block are not permitted.

Hence, an important enhancement of the original DDD code is to improve the deformation results and refine the stress distribution inside blocks by introducing finite elements into the blocks. A more accurate stress/strain distribution and higher computational efficiency can be achieved by considering a continuum material than those that can be achieved by the traditional DDA. In addition, the ability of an intact block to fracture is given because a block may contain a group of finite elements. Figure 2 shows the difference between the refined DDD method and the original DDD method. Clearly, Fig. 2a shows that in the original DDD method, the analysis region is divided into the DDA and FEM domains, and the mechanical contacts can happen along the edges of blocks in the DDA domain and the boundaries between these two domains. But for the proposed method, the mechanical contacts can only happen along the boundaries of the deformable blocks that contain numerous finite elements, as shown in Fig. 2b. The edges of the damaged elements represent newly formed joints, and sliding and opening may occur along these new joints. An intact block may rupture into several blocks,

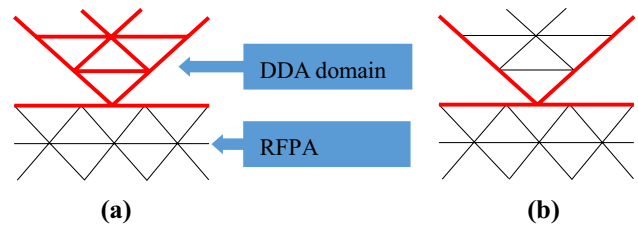


Fig. 2 Difference between a the original DDD method and b the proposed method (note: red lines denote the contact edges). (Color figure online)

and these smaller blocks can interact with each other. However, a block containing only one finite element is undividable. In the proposed method, the region of interest is analyzed using a unified formulation, and rock-like quasi-brittle materials can transform from continuum into discontinuum materials when the failure criteria are triggered. Consequently, the newly developed coupled method realizes the entire process simulation from continuum to discontinuum with high accuracy and efficiency. The calculation process of the new method is shown in Fig. 3.

3 Numerical Benchmarks

3.1 Cantilever Beam

In this section, a cantilever bending test is conducted to verify the elastic performance of the proposed method. In

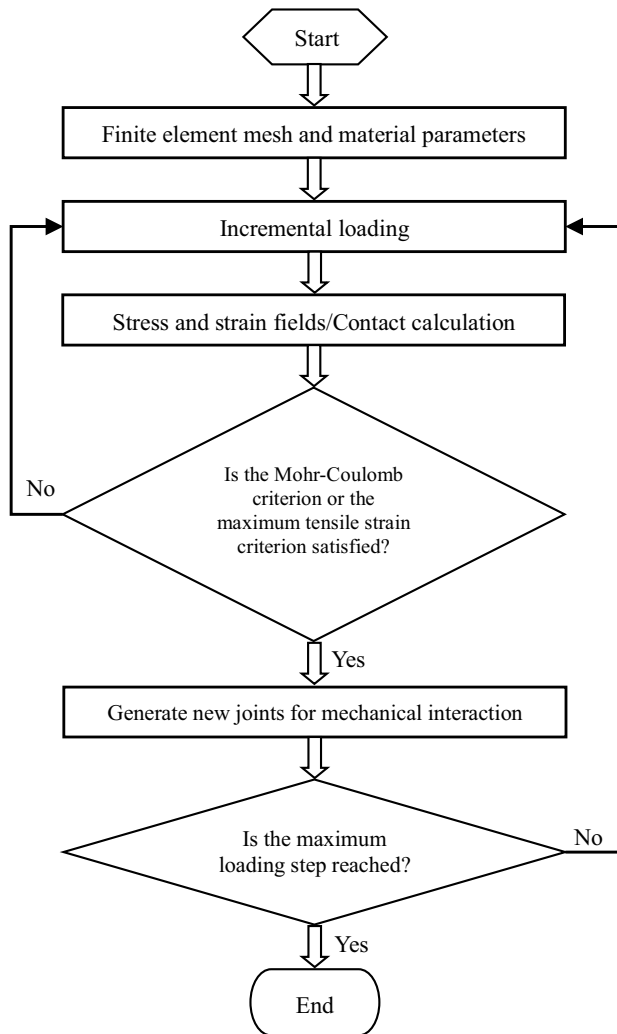


Fig. 3 Flowchart of the proposed method

this test, the elastic deformation accuracy and the influence of element number on the calculation are considered. The length and height of the cantilever beam are 0.04 m and 0.01 m, respectively (as shown in Fig. 4). The material is considered to be homogeneous, isotropic and elastic. For the elastic parameters, the elastic modulus is 10 GPa and Poisson's ratio is 0.3. The left side of the beam is fixed in all directions. Simultaneously, a point load of 10 kN is applied at the right end of the beam. The cantilever beam is discretized by traditional triangular elements. Four models (i.e., models I, II, III and IV) that contain different numbers of elements are considered.

The simulation results are shown in Fig. 5. A model containing more elements leads to greater deformation and more accurate results, as expected. Both models I and II result in poor beam deflections, mainly because of the effect of the number of elements on the accuracy of the integration scheme mentioned previously. Model III gives relatively acceptable results with a smaller error. With an increasing number of elements, the deflection curve of model IV nearly coincides with the theoretical curve. Therefore, the bending capacity and elastic performance of the novel coupled method are verified to be mainly controlled by the number of elements.

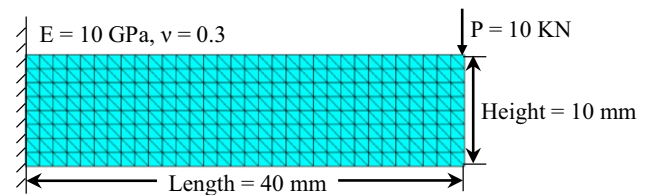


Fig. 4 Model configuration

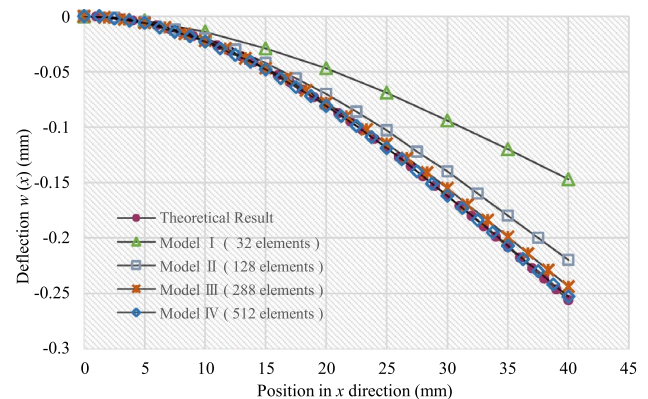


Fig. 5 Deflection along the middle line of the beam obtained using the proposed models

3.2 Sliding Block

A sliding test is performed to validate the coupled method in terms of the displacement calculation and dynamic contact capability. As shown in Fig. 6, two linearly elastic triangular blocks (blocks I and II) are considered. The density ρ of the material is 2600 kg/m^3 , and the acceleration coefficient of gravity g is 10 m/s^2 . The friction coefficient and incline angle of the surface between the two blocks are 0° and 30° , respectively. The time interval of the computation is 0.001 s , and the total computing time is 1.5 s . The left side and bottom of Block I are fixed in all directions. In the beginning of the simulation, block II statically rests on top of block I; then, block II starts to move downward along the interface under the force of gravity. The stress distribution of σ_y (the stress component along the y-axis) during sliding is shown in Fig. 7. Moreover, the displacement data for block II, obtained by the proposed method, are compared with the analytical solutions. The theoretical formulas are obtained based on kinematics and Newton’s laws of motion given below:

$$u_x = \frac{1}{2} \cdot g \cdot \cos \theta \cdot \sin \theta \cdot t^2, \tag{13}$$

$$u_y = \frac{1}{2} \cdot g \cdot \sin^2 \theta \cdot t^2. \tag{14}$$

Figure 8a, b shows that the computed displacements of block II along the x - and y -axes of the proposed method are entirely consistent with the theoretical solutions, and the ability of the proposed method to simulate displacement under dynamic contact is satisfactory.

3.3 Brazilian Disk Test

As an alternative to the direct uniaxial tensile test, which is difficult to perform at acceptable standards for rock-like quasi-brittle materials, the Brazilian disk test has a strong practical demand. Provided that the mechanical behavior of

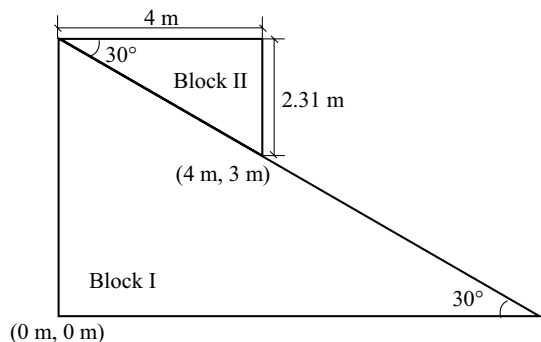


Fig. 6 Model geometry

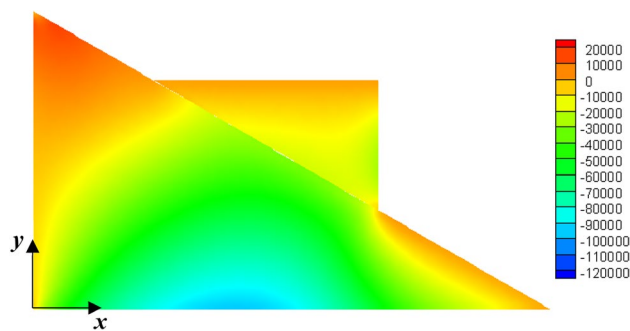
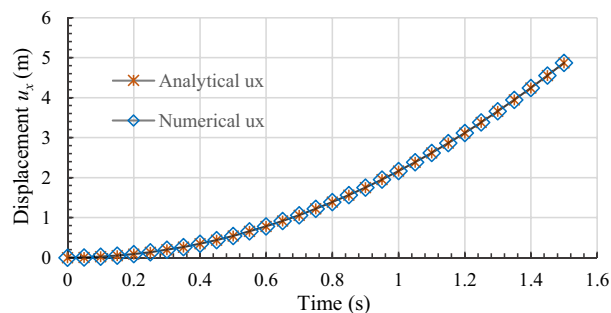


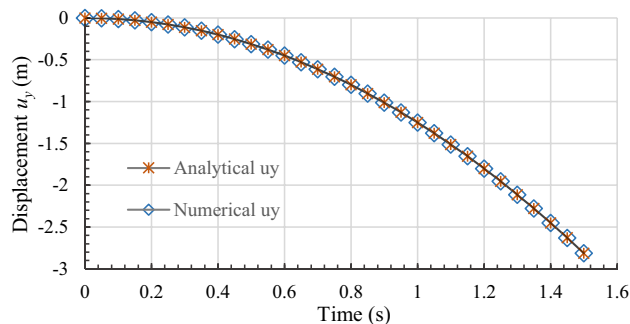
Fig. 7 The stress component σ_y computed by the proposed method at $t=0.993 \text{ s}$ (unit: Pa)

a material is perfectly linear-elastic until the point of failure, the tensile strength can be determined when a rock disk is under diametral compression. Hence, the Brazilian disk test is performed to verify the performance of the proposed method in terms of tensile strength and failure. Considering that a high stress concentration may lead to the failure of the load ends, the flattened Brazilian test is applied, namely the load ends of the rock disk are made flat to ensure that failure first occurs at the center of the model.

Figure 9 schematically shows the flattened Brazilian disk test and the geometry of the numerical specimen, in which P is the diametral loading and 2α and R are the loading angle and radius of the specimen, respectively. The thickness t is



(a) Horizontal displacement component u_x



(b) Vertical displacement component u_y

Fig. 8 Displacement of block II obtained by the proposed method

one unit. For the mechanical parameters of the material, the elastic modulus is 20 GPa, Poisson's ratio is 0.2 and the tensile strength is 2 MPa. The specimen is made up of 18,124 triangular elements.

Before the load value P peaks, the sample behaves linearly and elastically. During this elastic stage, the stress components along the x - and y -axes are distributed in a representative way, as shown in Fig. 10, in which the stress value is positive when towards the positive direction of the coordinate axis. With an increase in the loading P , the elements at the centre of the model first satisfy the strength criterion when $P=167.12$ kN. Thus, the simulated material strength is 2.128 MPa ($P/\pi tR$), which is slightly higher than the input tensile strength. If the peak load is maintained, then fractures quickly develop towards the upper and lower load ends. The initiation and propagation of the crack are illustrated in Fig. 11, in which the

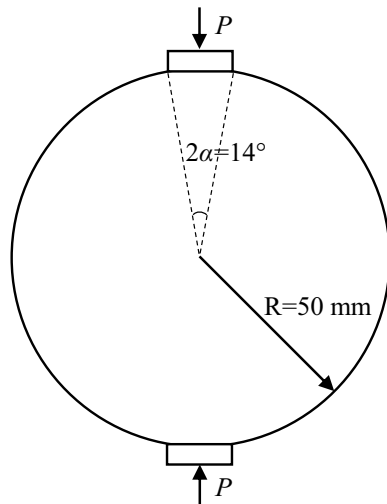


Fig. 9 Model configuration of the Brazilian disk test

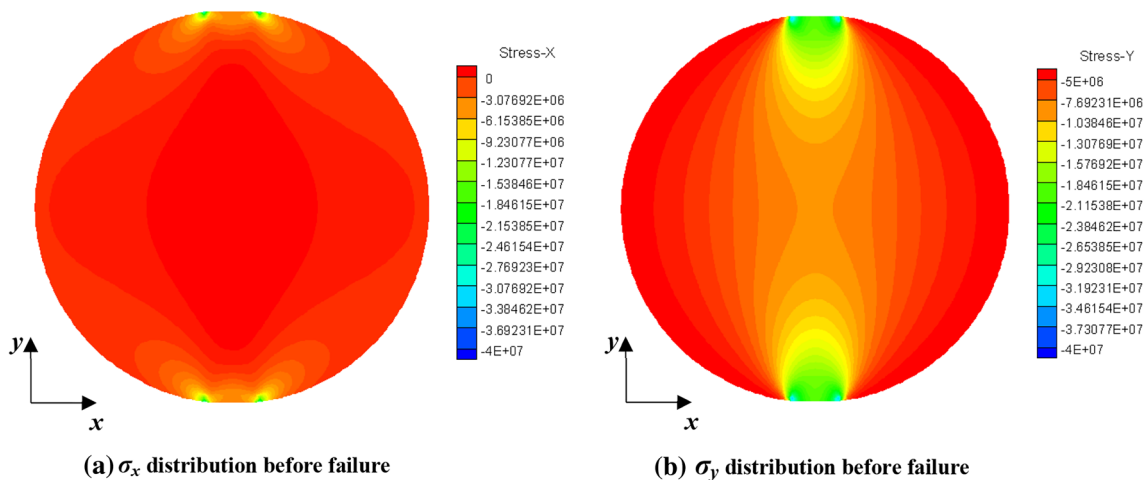


Fig. 10 Simulated stress fields of the Brazilian disk (unit: Pa)

red elements represent the damaged material and the straight solid lines (i.e., the boundaries of the red elements) represent the contact edges. The simulated failure modes are in good agreement with those observed in a previous study (Li et al. 2017) and experimental observations (Yuan and Shen 2017), as shown in Fig. 12.

Additionally, the critical elastic stress values along the vertical diameter of the rock disk are compared with the analytical solutions obtained according to the following equations given by Huang et al. (2015):

$$\sigma_x = \frac{P}{\pi \cdot R \cdot t \cdot \sin \alpha} \left(\frac{B_1}{A_1} + C_1 + \frac{B_2}{A_2} + C_2 \right) + \frac{P \cdot \cos \alpha}{\pi \cdot R \cdot t}, \quad (15)$$

$$\sigma_y = \frac{-P}{\pi \cdot R \cdot t \cdot \sin \alpha} \left(\frac{B_1}{A_1} - C_1 + \frac{B_2}{A_2} - C_2 \right) + \frac{P \cdot \cos \alpha}{\pi \cdot R \cdot t}, \quad (16)$$

where

$$A_1 = (R \cdot \cos \alpha + y)^2 + (R \cdot \sin \alpha)^2,$$

$$A_2 = (R \cdot \cos \alpha - y)^2 + (R \cdot \sin \alpha)^2,$$

$$B_1 = (R \cdot \cos \alpha + y) \cdot R \cdot \sin \alpha,$$

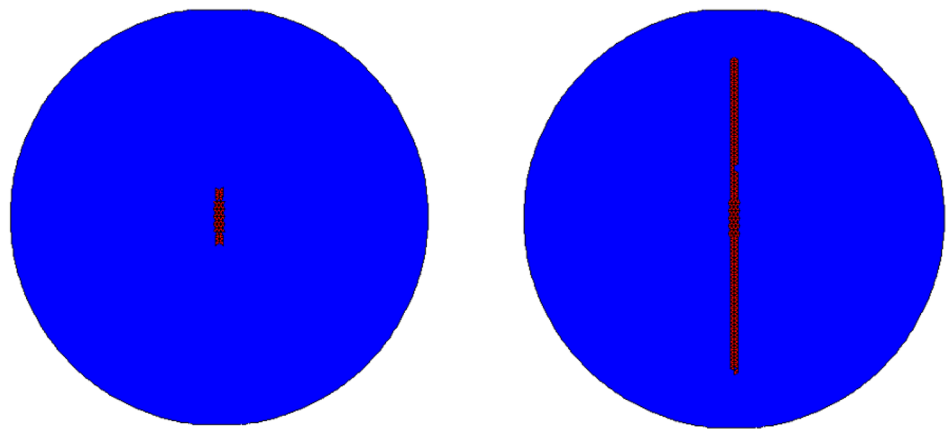
$$B_2 = (R \cdot \cos \alpha - y) \cdot R \cdot \sin \alpha$$

$$C_1 = -\arctan[(R \cdot \sin \alpha)/(R \cdot \cos \alpha + y)],$$

$$C_2 = -\arctan[(R \cdot \sin \alpha)/(R \cdot \cos \alpha - y)].$$

After normalization by $P/\pi tR$, a comparison between the simulated stresses and the theoretical stresses is shown in Fig. 13. Figure 13 illustrates that the elastic behavior of the Brazilian disk is well modelled by the proposed coupled method. Although there are stress differences at the upper

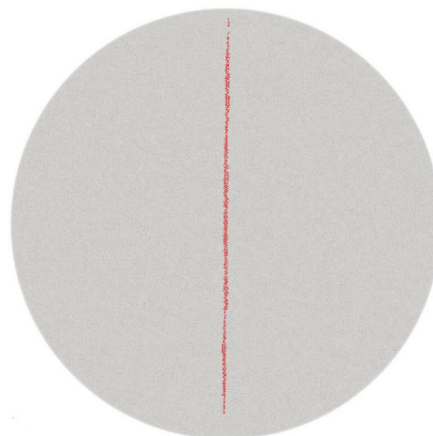
Fig. 11 Failure of the Brazilian disk by the proposed method



(a) Crack initiation in the middle

(b) Crack propagation along the diameter

Fig. 12 Failure modes obtained by **a** the PNMM method (Li et al. 2017) and **b** the related experiment (Yuan and Shen 2017)



(a)



(b)

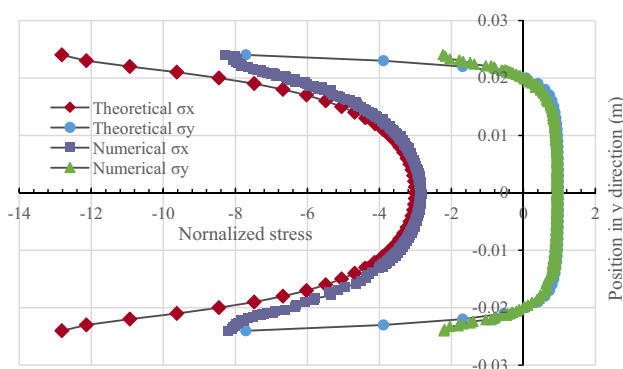


Fig. 13 Non-dimensional horizontal stress σ_x and vertical stress σ_y along the compressed diameter

and lower bounds because of the end effect, the simulated and theoretical stresses in the y and x directions (σ_x and σ_y) almost coincide at the central line. Therefore, the proposed

method is effective and valid for simulating the elastic stress field, strength and failure of rock-like materials.

3.4 Uniaxial Compression

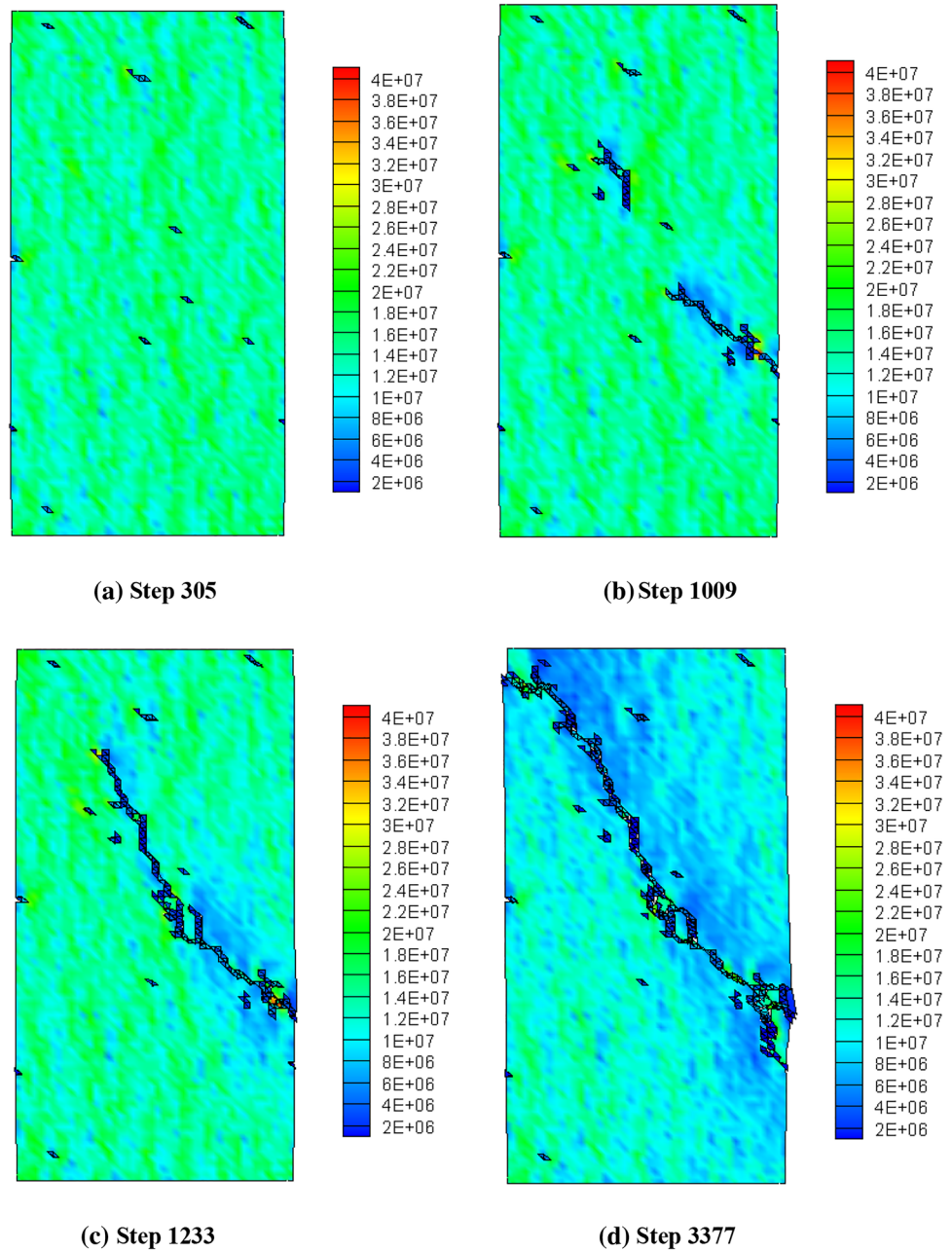
To validate the ability of the proposed method to model crack initiation, propagation and coalescence, a 2D rectangular specimen subjected to uniaxial compression is adopted. The dimension of the specimen is 150 mm in height and 75 mm in width. As mentioned above, heterogeneity is a typical feature of rock masses and has a significant influence on the failure process and strength characteristics of rock-like materials. Hence, the heterogeneity of the material is taken into account in this section, and the related mechanical parameters (i.e., the elastic modulus, cohesion and uniaxial tensile strength) are assumed to obey a given Weibull distribution, as listed in Table 1. The entire model consists of 8100 triangular elements. To simulate quasi-static or static loading conditions, the bottom of the specimen is fixed in

the vertical direction, and the top of the specimen is set to

Table 1 Mechanical properties of the rock specimen

Mechanical properties	Value
Material density ρ (kg/m ³)	2700
Elastic modulus E (GPa)	50
Poisson's ratio ν	0.2
Homogeneity index m	1.5
Cohesion c (MPa)	100
Internal friction angle φ (°)	20
Uniaxial tensile strength f_{t0} (MPa)	7

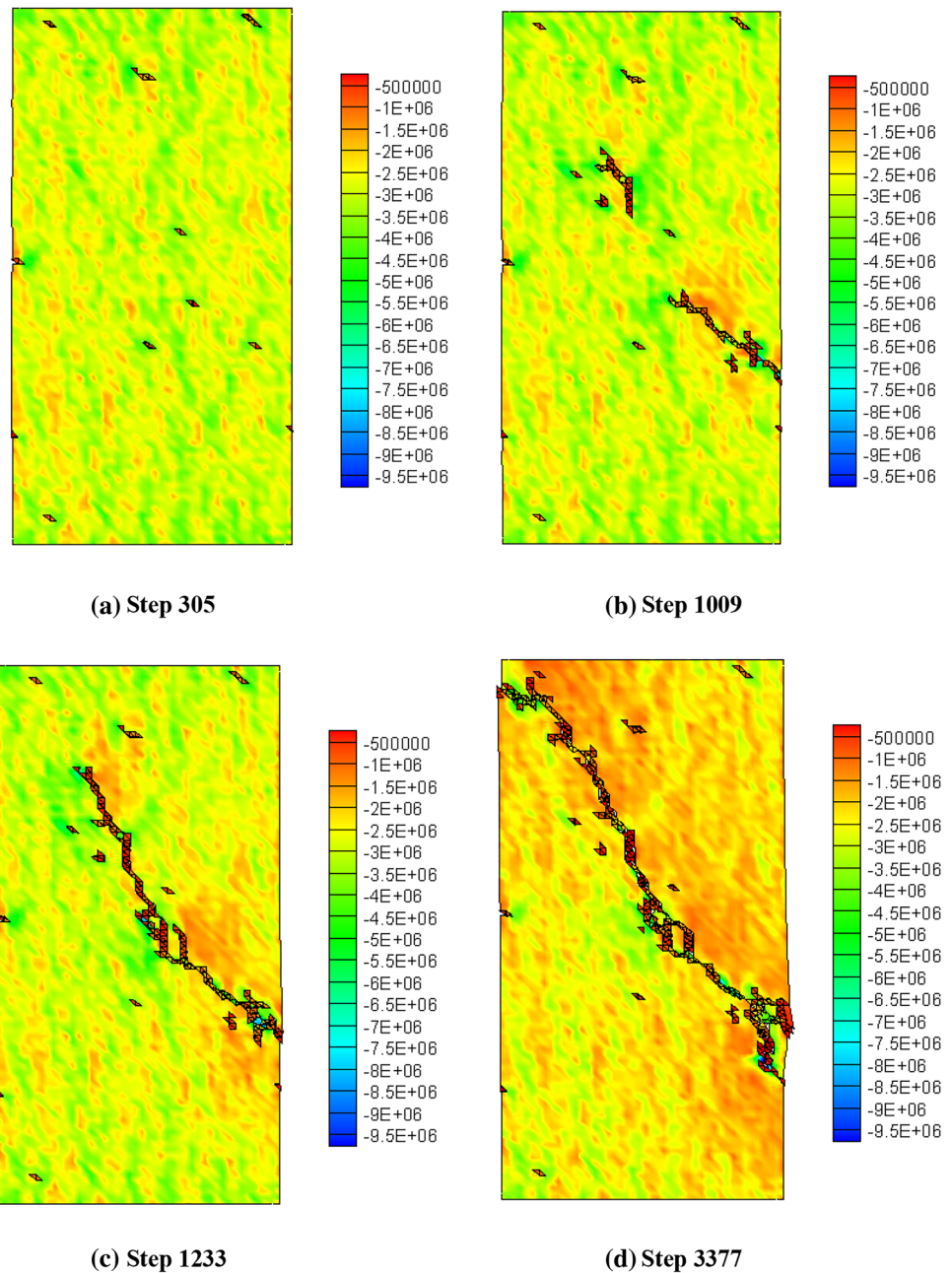
Fig. 14 Distribution of the major principal stress σ_1 (unit: Pa)



move downward at a constant rate of 0.02 mm/s, at which the dynamic effect can be neglected (Ha et al. 2015; Li and Wong 2012).

Figures 14 and 15 show the microcrack generation and growth processes within the sample at different stages. Figures 14a and 15a show that during the initial stage of the displacement loading, several finite elements become damaged at material defects due to their nonuniform distribution. These damage sites form the potential initiation locations of cracks and may induce crack propagation. Figures 14b and 15b show two separate cracks, one generated in the lower right and the other in the upper left parts of the specimen. In particular, the areas of high stress

Fig. 15 Distribution of the minor principal stress σ_3 (unit: Pa)



concentration occur at the corners of the upper left crack, causing the crack to develop both upwards and downwards. As new failures form, the concentrated stress will release and transfer. Under appropriate conditions, the stress may again increase at the ends of the crack, and the processes of stress build-up, stress relaxation and stress transfer induce the crack to develop gradually. Figures 14c and 15c illustrate that with increasing load, the previously formed cracks connect. Moreover, a small isolated rock body forms in the middle of the fracture, and the high-stress

areas concentrate to the lower right side of the fracture because of the relatively strong material strengths there. Figures 14d and 15d show that after the coalescence of the two main cracks, the newly formed fracture continues to develop towards the upper left, ultimately splitting the sample into two main blocks. In addition, the two blocks slide along the contact surface. The simulated failure process and pattern agree well with the results of previous studies (Wang et al. 2017; Tang et al. 2000).

4 Conclusion

The original DDD method is more suitable for simulating instantaneous instabilities involving massive movement processes, such as slope sliding or toppling, which will definitely put limitations on the application of the DDD method. Thus, in this paper, the previous DDD code was greatly refined based on the statistical damage theory and contact mechanics, and a novel coupled FEM/DDA method was then proposed to model the rock failure process from continuum to discontinuum. By hybridizing the FEM and DDA methods, the proposed coupled method inherited the advantages of both methods and is able to provide a complete and unified description of the entire rock deformation process (including crack initiation and propagation) and rock body movement (including translation, rotation and interaction), representing a distinct improvement over the conventional FEM, DDA and DDD methods.

In this study, to improve the deformation results and refine the stress distribution within blocks, finite elements are introduced into the blocks. Simultaneously, the ability of an intact block to fracture is determined by these finite elements, i.e., deformable blocks that contain several finite elements may split into smaller pieces if the strength criteria are satisfied continuously. The boundaries of damaged elements represent newly formed joints, and sliding and opening may occur along the new joints, i.e., mechanical interaction is allowed between adjacent blocks. All of these enhancements will extend the application range of the refined DDD method considerably.

Additionally, the correctness and validity of the proposed method were verified through a series of benchmark tests. The stress field, bending deformation, dynamic sliding, and strength characteristics and crack propagation were further analyzed to validate the effectiveness of the code. The simulated results were found to be consistent with the analytical solutions, previous studies and experimental observations. In conclusion, for the proposed coupled FEM/DDA method, the analysis region was modelled using a unified formulation, allowing rock-like quasi-brittle materials to transform from continuum into discontinuum materials when the failure criteria are triggered in the model. Although many challenges remain, the proposed method provides an effective and reliable approach for modelling the entire rock failure process with satisfactory accuracy.

Acknowledgements The work presented in this paper is financially supported by the National Natural Science Foundation of China (Grant nos. 51579031 and 51628401), the ARC Future Fellowship (Grant no. FT140100019), the ARC Discovery Project (Grant no. DP140100509) and the China Scholarship Council (Grant no. 201606060082). The authors are very grateful for the support.

References

- Bao H, Zhao Z (2013) Modeling brittle fracture with the nodal-based discontinuous deformation analysis. *Int J Comput Methods* 10(6):1350040
- Barla M, Piovano G, Grasselli G (2012) Rock slide simulation with the combined finite-discrete element method. *Int J Geomech* 12(6):711–721
- Basu B, Tiwari D, Kundu D, Prasad R (2009) Is Weibull distribution the most appropriate statistical strength distribution for brittle materials? *Ceram Int* 35(1):237–246
- Brady BHG, Bray JW (1978) The boundary element method for determining stress and displacements around long openings in a triaxial stress field. *Int J Rock Mech Min Sci Geomech Abstr* 15(1):21–28
- Cundall PA (1971) A computer model for simulating progressive large scale movements in blocky rock systems. In: *Proceedings of the symposium of the international society for rock mechanics (ISRM)*, Nancy, France, pp 129–136
- Fallah NA, Bailey C, Cross M, Taylor GA (2000) Comparison of finite element and finite volume methods application in geometrically nonlinear stress analysis. *Appl Math Model* 24(7):439–455
- Gong B, Tang CA (2016) Slope-slide simulation with discontinuous deformation and displacement analysis. *Int J Geomech* 17(5):E4016017
- Gong B, Wang SY, Sloan SW, Sheng DC, Tang CA (2018) Modelling coastal cliff recession based on the GIM-DDD method. *Rock Mech Rock Eng* 51(4):1077–1095
- Ha YD, Lee J, Hong JW (2015) Fracturing patterns of rock-like materials in compression captured with peridynamics. *Eng Fract Mech* 144:176–193
- Hoxha D, Homand F (2000) Microstructural approach in damage modelling. *Mech Mater* 32:377–387
- Huang YG, Wang LG, Chen JR, Zhang JH (2015) Theoretical analysis of flattened Brazilian splitting test for determining tensile strength of rocks. *Chin J Rock Soil Mech* 36(3):739–748 (in Chinese)
- Hudson JA, Harrison JP (1997) *Engineering rock mechanics: an introduction to the principles*. Pergamon, Oxford
- Jiao Y, Zhang XL, Zhao J (2012) Two-dimensional DDA contact constitutive model for simulating rock fragmentation. *J Eng Mech* 138(2):199–209
- Jing L (2003) A review of techniques, advances and outstanding issues in numerical modelling for rock mechanics and rock engineering. *Int J Rock Mech Min Sci* 40(3):283–353
- Jing L, Stephansson O (2007) Implicit discrete element method for block systems-discontinuous deformation analysis (DDA). In: Jing L, Stephansson O (eds). *Developments in geotechnical engineering*. Elsevier, Amsterdam, pp 317–364
- Krajcinovic D, Silva MAG (1982) Statistical aspects of the continuous damage theory. *Int J Solids Struct* 18(7):551–562
- Li H, Wong LN (2012) Influence of flaw inclination angle and loading condition on crack initiation and propagation. *Int J Solids Struct* 49(18):2482–2499
- Li G, Liang ZZ, Tang CA (2015) Morphologic interpretation of rock failure mechanisms under uniaxial compression based on 3D multiscale high-resolution numerical modeling. *Rock Mech Rock Eng* 48(6):2235–2262
- Li X, Zhang QB, He L, Zhao J (2017) Particle-based numerical manifold method to model dynamic fracture process in rock blasting. *Int J Geomech* 17(5):E4016014
- Liang ZZ, Tang CA, Li HX, Zhang YB (2004) Numerical simulation of 3D failure process in heterogeneous rocks. *Int J Rock Mech Min Sci* 41(s1):323–328
- Manthei G (2005) Characterization of acoustic emission sources in a rock salt specimen under triaxial compression. *Bull Seismol Soc Am* 95:1674–1700

- Meglis IL, Chow TM, Young RP (1995) Progressive microcrack development in test on Lac du Bonnet: I. Emission source location and velocity measurements. *Int J Rock Mech Min Sci Geomech Abstr* 32(8):741–750
- Ning Y, Zhao Z (2013) A detailed investigation of block dynamic sliding by the discontinuous deformation analysis. *Int J Numer Anal Methods Geomech* 37(15):2373–2393
- Rutqvist J, Børgesson L, Chijimatsu M, Kobayashi A, Jing L, Nguyen TS, Noorishad J, Tsang CF (2001) Thermo-hydro-mechanics of partially saturated geological media: governing equations and formulation of four finite element models. *Int J Rock Mech Min Sci* 38(1):105–127
- Shi GH (1988) *Discontinuous deformation analysis: a new numerical model for the statics and dynamics of block systems*. University of California, Berkeley
- Shi GH (2015) Contact theory. *Sci China Technol Sci* 58(9):1450–1496
- Strouboulis T, Babuška I, Copps K (2000) The design and analysis of the generalized finite element method. *Comput Methods Appl Mech Eng* 181:43–69
- Tang CA (1997) Numerical simulation of progressive rock failure and associated seismicity. *Int J Rock Mech Min Sci* 34(2):249–261
- Tang CA, Hudson JA (2002) Understanding rock failure through numerical simulations and implications for the use of codes in practical rock engineering. In: Hammah R, Bawden W, Curran J, Telesnicki M (eds). *Proceedings of the 5th North American rock mechanics symposium and the 17th tunnelling association of Canada conference*, Toronto, Canada, pp 705–712
- Tang CA, Liu H, Lee PKK, Tsui Y, Tham LG (2000) Numerical studies of the influence of microstructure on rock failure in uniaxial compression—Part I: effect of heterogeneity. *Int J Rock Mech Min Sci* 37:555–569
- Tang CA, Tang SB, Gong B, Bai HM (2015) Discontinuous deformation and displacement analysis: from continuous to discontinuous. *Sci China Technol Sci* 58(9):1567–1574
- Wang SY, Sloan SW, Huang ML, Tang CA (2011) Numerical study of failure mechanism of serial and parallel rock pillars. *Rock Mech Rock Eng* 44(2):179–198
- Wang YT, Zhou XP, Shou YD (2017) The modeling of crack propagation and coalescence in rocks under uniaxial compression using the novel conjugated bond-based. *Int J Mech Sci* 128–129:614–643
- Weibull W (1951) A statistical distribution function of wide applicability. *J Appl Mech* 18:293–297
- Yuan R, Shen B (2017) Numerical modelling of the contact condition of a Brazilian disk test and its influence on the tensile strength of rock. *Int J Rock Mech Min Sci* 93:54–65

Publisher's Note Springer Nature remains neutral with regard to jurisdictional claims in published maps and institutional affiliations.